

Effects of T-tubules on dielectric spectra of skeletal muscle simulated by boundary element method with two-dimensional models

メタデータ	言語: eng 出版者: 公開日: 2017-10-03 キーワード (Ja): キーワード (En): 作成者: メールアドレス: 所属:
URL	http://hdl.handle.net/2297/3893

Effects of T-tubules on dielectric spectra of skeletal muscle simulated by
boundary element method with two-dimensional models

Katsuhisa Sekine ^{a,*}, Chiharu Hibino ^a, Miyuki Kimura ^a, and Koji Asami ^b

^a *School of Health Sciences, Faculty of Medicine, Kanazawa University, 5-11-80 Kodatsuno,
Kanazawa, 920-0942, Japan*

^b *Institute for Chemical Research, Kyoto University, Uji, Kyoto 611-0011, Japan*

* Corresponding author. Fax: +81-76-234-4366.

E-mail address: sekine@kenroku.kanazawa-u.ac.jp (K. Sekine)

Abstract

In order to investigate the origin of large intensity the α -relaxation in skeletal muscles observed in dielectric measurements with extracellular electrode methods, effects of the interfacial polarization in the T-tubules on dielectric spectra were evaluated with the boundary-element method using two-dimensional models in which the structure of the T-tubules were represented explicitly. Each model consisted of a circular inclusion surrounded by a thin shell corresponding to the sarcolemma. The T-tubules were represented by simplified two types of invagination of the shell: straight invagination along the radial directions, and branched one. Each of the models was subjected to two kinds of calculations relevant to experiments with the extracellular and the intracellular electrode methods. Electrical interactions between the cells were omitted in the calculations. The both calculations showed that the dielectric spectra of the models contained two relaxation terms. The low-frequency relaxation term assigned to the α -relaxation depended on the structure of the T-tubules. Values of the relaxation frequency of the α -relaxation obtained from the two types of calculations agreed with each other. At the low-frequency limit, the permittivity obtained from the extracellular-electrode-type calculations varied in proportion to the capacitance obtained from the intracellular-electrode-type ones. These results were consistent with conventional lumped and distributed circuit models for the T-tubules. This confirms that the interfacial polarization in the T-tubules in a single muscle cell is not sufficient to explain the experimental results in which the intensity of the α -relaxation in the extracellular-electrode-type experiments exceeded the intensity expected from the results of the intracellular-electrode-type experiments. The high-frequency relaxation term that was assigned to the β -relaxation was also affected by the T-tubule structure in the calculations relevant to the extracellular-electrode-type experiments.

Keywords:

Boundary element method; Complex permittivity; Dielectric relaxation; Interfacial polarization; Muscle cell; T-tubule

1. Introduction

Dielectric spectra of cells and tissues have been of interest in physiology, biophysics and bioengineering because those serve as fundamentals not only for understanding their electrical phenomena including effects of electromagnetic fields, but also for developing electromagnetic techniques for analyzing cells, tissues and bodies [1-9]. According to Schwan's survey [1], the dielectric spectra have three types of dielectric relaxation that appear in different frequency regions of the applied ac electric fields: α -relaxation below a few kHz, β -relaxation between 1 kHz and 1 GHz, and γ -relaxation above 1 GHz. The γ -relaxation is due to orientation of water molecules. The β -relaxation is attributed to interfacial polarization caused by accumulation of charges at boundaries between the membranes and the aqueous phases. For the α -relaxation, several possible polarization mechanisms have been proposed, which are due to (1) displacement of counterions surrounding charged membranes [1, 5], (2) interfacial polarization related to peculiar cell structures such as the T-tubules in skeletal muscles [10, 11], gap junctions between cells [12, 13], and small holes in the cell membrane [14], and (3) gating of ion permeation in excitable membranes [15, 16]. As an extended view, Dissado reexamined the mechanism of the three relaxation terms based on fractal structures in tissues [17]. At this stage, the mechanism of the α -relaxation has not been made clear because of difficulties in measurements in the low frequency region chiefly due to interference from electrode polarization [18, 19], and the structural complexities of cells and tissues.

The electrical properties of skeletal muscles have been investigated by the extracellular electrode (EE) [1-10] and the intracellular electrode (IE) [2, 4, 11, 20, 21] methods. The EE method, which is commonly used for dielectric spectroscopy, measures the whole cells between electrodes, whereas, in the IE method, one of electrodes is placed inside of the cell to make measurements across the cell membrane. In 1954, Schwan [22] reported the dielectric spectra of skeletal muscles measured by the EE method between 20 Hz to 200 kHz, and showed that these included two relaxation terms located near 100 Hz (α -relaxation) and above 100 kHz (β -relaxation). In his review paper in 1957 [1], he analyzed the α -relaxation following O'Konski's theory [23] and, from analogy with the α -relaxation found for lysed erythrocytes and polystyrene spheres, concluded that the α -relaxation was attributed to

the counterion polarization. The β -relaxation was reasonably explained by the interfacial polarization related to the membrane at the outer surface of the muscle cells (the sarcolemma). Subsequently in 1964, Fatt and Falk carried out the measurements by the EE [10] and by the IE [11] methods and found two relaxation terms in both of the experiments. Based on these results, they proposed that these relaxation terms were both caused by the interfacial polarization in which the effects of the tubular system in the skeletal muscles were represented by circuits consisting of capacitors and resistors connected in series. The simplest circuit is the lumped circuit model (LCM) for the T-tubules [20, 21]. This is a serial combination of a capacitor due to the whole T-tubule membrane and a resistor representing the access resistance. A parallel combination of the LCM for the T-tubules and a capacitor corresponding to the sarcolemma provides the apparent electrical properties of the cell membrane. According to this model, the α - and the β -relaxation are attributable to the T-tubules and the sarcolemma, respectively.

Arguments about the mechanism of the α -relaxation of the skeletal muscles arise from the disagreement about its intensity between the results of the IE-type experiments and those of the EE-type ones. According to the discussion by Foster and Schwan [5], the relaxation frequency of the α -relaxation in the EE-type experiments agrees with that for the apparent capacitance of the cell membrane derived from the IE-type experiments, on the other hand, the intensity of the α -relaxation is much larger than that expected from the increase in the apparent capacitance of the cell membrane due to the T-tubules. Because of the disagreement about the relaxation intensity, they argued that, in addition to the interfacial polarization in the T-tubules, the counterion polarization mechanism is required to explain the behavior of the α -relaxation. However, validity of this discussion should be examined because it is based on conventional theoretical formulas in which the morphological effects are considered implicitly. It is accepted to be reasonable to derive theoretical formulas for the interfacial polarization in cell suspensions by solving Laplace's equation by taking account of the morphology and electrical properties of cells [24-27]. In the conventional theoretical formulas for the skeletal muscles, however, a cell was assumed to be covered with a smooth membrane whose electrical properties were determined from the LCM for T-tubules to incorporate their contributions

[10, 28]. This approach is a kind of expedients caused by the complex cell morphology for which Laplace's equation cannot be solved analytically. In recent theoretical studies of composites and cell suspensions [29, 30], Laplace's equation was solved numerically to show the morphological effects explicitly. This approach provided information that was not obtained with the conventional analytical methods. The morphology of the skeletal muscles subjected to the EE-type experiments is characterized by the network of the T-tubules in each of the cells and the anisotropic structure of the tissue consisting of bundles of the elongated cells. To derive the conclusion of the mechanism of the α -relaxation in the EE-type experiments, it is necessary to examine the validity of the conventional analytical formulas from the comparison with the results of numerical calculations in which the morphology of the skeletal muscles is represented explicitly.

As the first stage of investigations based on the numerical calculations for the skeletal muscles, we examined whether the interfacial polarization in the T-tubules causes the same effects in the EE- and the IE-type experiments, using two-dimensional models in which the T-tubules were represented by simplified local deformation of the cell membrane. The use of the two-dimensional models in the calculations relevant to the EE-type experiments is the same approach as that adopted by Fatt [10], and corresponds to experimental conditions in which the external electric fields are directed perpendicular to the muscle fibers. Electrical interaction between the cells due to the bundle structure was omitted. In addition to the comparison between the EE- and the IE-type calculations, validity of the conventional equivalent electric circuit models for the T-tubules was examined.

2. Models and methods of calculations

2.1. Cell models

From the three-dimensional viewpoint, the muscle fiber and the T-tubules were modeled, respectively, by a cylinder and trenches on the side of the cylinder, where the external electric fields were directed perpendicular to the cylinder. Figures 1 and 2 show the two-dimensional view of the models. The muscle fiber is represented as a circular inclusion $10\ \mu\text{m}$ in radius, a_s , surrounded by a thin shell $10\ \text{nm}$ in thickness, T_s . Although the value of a_s ($a_s = 10\ \mu\text{m}$) is somewhat smaller than those

used in previous theoretical simulations [28, 31], it is still realistic. The T_s value ($T_s = 10$ nm) was chosen for a practical reason to simplify the calculations, and is larger than the thickness of the hydrophobic region in cell membranes ranging from 4 to 5 nm [2-4]. The T-tubules are arranged symmetrically. The number of the tubules, N_T , is two in models A2 and B2, four in models A4, B4 and C4, and eight in model A8. Width of the tubules, W_T , is made uniform. As shown in Fig. 2, the tubules are straight invaginations of depth D_T directed toward the center of the circle in A-type models (A2, A4 and A8). In B-type models (B2 and B4), each tubule is divided into two branches of azimuth θ_T . Effects of the tubule structure on the dielectric spectra were examined by changing N_T , W_T , D_T , and θ_T systematically, as shown in Table 1. The values of W_T from 50 to 200 nm are of the same order as the T-tubule diameter [32]. Model C4 relevant to a detubulated muscle fiber [4, 21] consists of the straight tubules ($N_T = 4$, $W_T = 50$ nm, $D_T = 8$ μ m) that are disconnected from the surface membrane by a space of 1 μ m. Model S without tubules was used for control calculations.

=== Fig. 1 ===

=== Fig. 2 ===

=== Table 1 ===

We adopted the following values for relative permittivity ε and conductivity κ of the inner (subscript i), outer (a), and shell (s) phases: $\varepsilon_i = \varepsilon_a = 80$, $\kappa_i = \kappa_a = 1$ S/m, $\varepsilon_s = 2$, and $\kappa_s = 0$. Effects of proteins and DNA on these electrical parameters [3-5] were omitted for simplicity. The values for ε_i and ε_a ($\varepsilon_i = \varepsilon_a = 80$), and that for ε_s ($\varepsilon_s = 2$) are compared to the permittivity of water and that of insulating non-polar materials, respectively [33]. The values for κ_i and κ_a are the same order as the conductivity of physiological saline solutions [34]. The tubular lumen was assumed to be filled with the external medium, to simplify the problems.

The assumptions about the parameter values adopted to simplify the calculations may provide some difficulties in comparing between the present theoretical study and previous experimental studies, however, are allowed in the comparison between the two types of calculations, which mimic the EE-

and the IE-type experiments.

2.2. Calculation of dielectric spectra

Dielectric spectra relevant to the EE-type experiments were calculated with a method similar to that used for three-dimensional models in our previous papers [35-38]. The procedure of the calculation consists of three steps. First, the electric potential ϕ_{EE} induced at $\mathbf{r}(x, y)$ around the model by an uniform external ac field $\mathbf{E}_{EE0}(E_{EE0x}, E_{EE0y})$ was evaluated by solving Laplace's equation using BEM with the Green function and the cubic shape functions for two-dimensional systems [39, 40]. Second, the complex polarization factors B_{EEx} and B_{EEy} for the model in x and y directions were evaluated by analyzing the resulting ϕ_{EE} using the relation

$$\phi_{EE} = \frac{S}{2\pi(x^2 + y^2)}(xE_{EE0x}B_{EEx} + yE_{EE0y}B_{EEy}), \quad (1)$$

where S denotes the area of the model approximated as $S = \pi a_s^2$. Third, the complex permittivity for the two-dimensional suspension of the model was calculated from the Wagner-type mixture equations [26] that were derived assuming no interaction between the models. If the models are randomly oriented, the complex permittivity of the suspension ε_{EE}^* is represented as

$$(\varepsilon_{EE}^* - \varepsilon_a^*)/(\varepsilon_{EE}^* + \varepsilon_a^*) = P(B_{EEx} + B_{EEy})/4, \quad (2)$$

where ε_a^* is the complex permittivity of the outer phase, and P is the area fraction of the models in the two-dimensional suspension. The complex permittivity is defined as $\varepsilon^* = \varepsilon + \kappa/(i\omega\varepsilon_0)$ with ε , κ , imaginary unit i , angular frequency ω represented as $\omega = 2\pi f$ using frequency f of the external ac electric field, and the permittivity of vacuum ε_0 . When $P \ll 1$, Eq. (2) is simplified, and, for convenience, is represented using new quantity ε_{EED}^* that is an increment in the complex permittivity of the suspension due to the models in the randomly oriented suspensions normalized by P , in the

following way:

$$\varepsilon_{\text{EED}}^* \equiv (\varepsilon_{\text{EE}}^* - \varepsilon_a^*)/P = \varepsilon_{\text{EEDx}}^* + \varepsilon_{\text{EEDy}}^*, \quad (3)$$

$$\varepsilon_{\text{EEDx}}^* = \varepsilon_a^* B_{\text{EEEx}}/2, \quad (4)$$

$$\varepsilon_{\text{EEDy}}^* = \varepsilon_a^* B_{\text{EEEy}}/2, \quad (5)$$

where $\varepsilon_{\text{EEDx}}^*$ and $\varepsilon_{\text{EEDy}}^*$ correspond to the normalized increments in the complex permittivity by the models oriented along x - and y -axis. The $\varepsilon_{\text{EED}}^*$ can be expressed as $\varepsilon_{\text{EED}}^* = \varepsilon_{\text{EED}}' - i\varepsilon_{\text{EED}}'' + \kappa_{\text{EED}}^{\text{L}}/(i\omega\varepsilon_0)$, where $\varepsilon_{\text{EED}}'$ is the real part of $\varepsilon_{\text{EED}}^*$. The imaginary part of $\varepsilon_{\text{EED}}^*$ includes two terms, $\varepsilon_{\text{EED}}''$ and $\kappa_{\text{EED}}^{\text{L}}/(\omega\varepsilon_0)$, where $\kappa_{\text{EED}}^{\text{L}}$ is the dc conductivity.

In the experiments with the IE method, the electrodes are placed inside and outside of the cell, and are connected to a generator and to the ground, respectively. To simulate this situation, we placed two concentric circles of radii a_{IEH} and a_{IEG} centered at $(0, 0)$ representing the electrode in the cell and the ground, respectively. The values of a_{IEH} and a_{IEG} were made to be $1 \mu\text{m}$ and $20 \mu\text{m}$, respectively, so that the shell phase of the models was placed between these circles. Under the boundary conditions that the potential V_{IEH} at the inner circle and that V_{IEG} at the outer one are fixed to be $1 V_{\text{PP}}$ and $0 V_{\text{PP}}$, respectively, Laplace's equation was solved to obtain the normal components of the electric fields at the surfaces of the circles with conventional BEM procedures [39, 40]. Using ε_i^* and the normal components of the electric fields at the inner circle, value of I_{IEH} , which is electric current per unit length along z -axis through the internal electrode, was obtained. Finally, complex capacitance C_{IE}^* for the model of unit length along z -axis was evaluated from $C_{\text{IE}}^* = I_{\text{IEH}}/[i\omega(V_{\text{IEH}} - V_{\text{IEG}})]$, and was represented using capacitance C_{IE} and conductance G_{IE} given by a relation $C_{\text{IE}}^* = C_{\text{IE}} + G_{\text{IE}}/(i\omega)$.

The calculations for model S were carried out with analytical methods using the cylindrical coordinate system [2, 41]. The B_{EEEx} and B_{EEEy} in the EE-type calculations for model S are represented as

$$B_{\text{EE}x} = B_{\text{EE}y} = 2 \frac{\varepsilon_q^* - \varepsilon_a^*}{\varepsilon_q^* + \varepsilon_a^*}, \quad (6)$$

$$\varepsilon_q^* = \varepsilon_s^* \frac{(1+\nu)\varepsilon_1^* + (1-\nu)\varepsilon_s^*}{(1-\nu)\varepsilon_1^* + (1+\nu)\varepsilon_s^*}, \quad (7)$$

$$\nu = (1 - T_s/a_s)^2, \quad (8)$$

where ε_q^* and ν are, respectively, the equivalent complex permittivity and the area fraction of inner phase within shelled circle for model S. Fatt represented the impedance the two-dimensional suspensions with circuit models [10]; one of these was a parallel combination of the outer medium and a composite circuit that was a series combination of the outer medium and an equivalent element for the cell. Using a similar circuit model, $\varepsilon_{\text{EED}}^*$ for model S given by Eqs. (3)-(6) can be represented as

$$\frac{\varepsilon_{\text{EED}}^*}{2} = \frac{2}{1/\varepsilon_a^* + 1/\varepsilon_q^*} - \varepsilon_a^*. \quad (9)$$

Since Eq. (7) can be modified into $1/\varepsilon_q^* = T_s/(a_s\varepsilon_s) + i\omega\varepsilon_0/\kappa_a$ under the conditions $\varepsilon_1 = \varepsilon_a$, $\kappa_1 = \kappa_a$, $\kappa_s = 0$, and $T_s/a_s \ll 1$ which are relevant to the present study, Eq. (9) can be represented by the following approximate relation:

$$\frac{\varepsilon_{\text{EED}}^*}{2} = \frac{1}{i\omega\varepsilon_0/\kappa_a + T_s/(2a_s\varepsilon_s)} - \frac{\kappa_a}{i\omega\varepsilon_0}. \quad (10)$$

This relation shows that model S exhibits one relaxation term attributable to the β -relaxation due to $[i\omega\varepsilon_0/\kappa_a + T_s/(2a_s\varepsilon_s)]^{-1}$ in the right side of Eq. (10). In the case of the IE-type,

$$\frac{1}{C_{\text{IE}}^*} = \frac{1}{2\pi\varepsilon_0} \left\{ \frac{\log_e [a_{\text{IEG}}/(a_s + T_s)]}{\varepsilon_a^*} + \frac{\log_e [(a_s + T_s)/a_s]}{\varepsilon_s^*} + \frac{\log_e (a_s/a_{\text{IEH}})}{\varepsilon_1^*} \right\}. \quad (11)$$

Similarly to the case of $\varepsilon_{\text{EED}}^*$, this relation can be modified into the following approximate form representing the β -relaxation:

$$\frac{1}{C_{\text{IE}}^*} = \frac{1}{2\pi\varepsilon_0} \left[\frac{i\omega\varepsilon_0 \log_e(a_{\text{IEG}}/a_{\text{IEH}})}{\kappa_a} + \frac{T_s}{a_s\varepsilon_s} \right]. \quad (12)$$

2.3. Equivalent circuit models for T-tubules

As an alternative approach to evaluate the effects of the T-tubules, the calculations were carried out using Eqs. (3)-(8) for model S, where ε_s^* was replaced by the equivalent complex permittivity $\overline{\varepsilon_s^*}$ of the shell phase including the effects of the T-tubules represented by equivalent circuit models shown in Fig. 3. The $\overline{\varepsilon_s^*}$ can be represented by $\overline{\varepsilon_s^*} = \varepsilon_s + N_T Y_T T_s / (i\omega 2\pi a_s \varepsilon_0)$, where Y_T is the admittance of each T-tubule per unit length along z -axis. The equivalent relative permittivity $\overline{\varepsilon_s}$ and conductivity $\overline{\kappa_s}$ of the shell phase are defined as $\overline{\varepsilon_s^*} = \overline{\varepsilon_s} + \overline{\kappa_s} / (i\omega\varepsilon_0)$, and are represented by the imaginary Y_T'' and the real Y_T' parts of Y_T as follows:

$$\overline{\varepsilon_s} = \varepsilon_s \left(1 + \frac{T_s}{2\pi a_s \varepsilon_s \varepsilon_0} \frac{N_T Y_T''}{\omega} \right), \quad (13)$$

$$\overline{\kappa_s} = \frac{T_s}{2\pi a_s} N_T Y_T'. \quad (14)$$

==== Fig. 3 ====

In the case of the limped-circuit model (LCM, Fig. 3(A)), where the capacitance C_T^{LCM} of the T-tubule membrane and the access resistance R_A^{LCM} are connected in series, Y_T becomes $1/Y_T = R_A^{\text{LCM}} + 1/(i\omega C_T^{\text{LCM}})$. Hence,

$$Y_T' = (\omega C_T^{\text{LCM}})^2 R_A^{\text{LCM}} / [1 + (\omega \tau_T^{\text{LCM}})^2], \quad (15)$$

$$Y_T'' = \omega C_T^{\text{LCM}} / [1 + (\omega \tau_T^{\text{LCM}})^2], \quad (16)$$

where τ_T^{LCM} is the relaxation time for the T-tubule represented as

$$\tau_T^{\text{LCM}} = 1/(2\pi f_T^{\text{LCM}}) = C_T^{\text{LCM}} R_A^{\text{LCM}}. \quad (17)$$

The f_T^{LCM} in this relation is the relaxation frequency for the T-tubule. The C_T^{LCM} corresponds to the membrane of the T-tubule, and is considered to be proportional to the tubule membrane area. Using the length of the each T-tubule in xy -plane, L_{TC} , which is given by $L_{\text{TC}} = D_T$ in A-type models and by $L_{\text{TC}} = D_T + 2(a_s - D_T)\theta_T$ in B-type ones, C_T^{LCM} is represented by

$$C_T^{\text{LCM}} = 2L_{\text{TC}}\epsilon_0\epsilon_s/T_s. \quad (18)$$

For the distributed-circuit model (DCM, Fig. 3(B)), we can derive formulas for Y_T following the transmission line theory [2, 4, 41] as described briefly in Appendix A. In the derivation, we assumed that the voltage and the current waves were perfectly reflected at the bottom of the tubules. In the case of the A-type models with straight T-tubules, Y_T is represented as

$$Y_T = Y_0^{\text{DCM}} \frac{1 - \exp(-2\gamma^{\text{DCM}} D_T)}{1 + \exp(-2\gamma^{\text{DCM}} D_T)}, \quad (19)$$

where Y_0^{DCM} is the reciprocal of the characteristic impedance Z_0^{DCM} , and γ^{DCM} is the propagation constant. The Y_0^{DCM} and γ^{DCM} are dependent on the specific capacitance c_T^{DCM} of the T-tubule membrane and the specific resistance r_L^{DCM} of the lumen per unit length of the T-tubules as follows:

$$(\gamma^{\text{DCM}})^2 = i\omega c_T^{\text{DCM}} r_L^{\text{DCM}}, \quad (20)$$

$$(1/Y_0^{\text{DCM}})^2 = (Z_0^{\text{DCM}})^2 = r_L^{\text{DCM}}/(i\omega c_T^{\text{DCM}}). \quad (21)$$

with

$$c_T^{\text{DCM}} = 2\varepsilon_0\varepsilon_s/T_s, \quad (22)$$

$$r_L^{\text{DCM}} = 1/(W_T\kappa_a). \quad (23)$$

In the case of the B-type models with branched tubules,

$$Y_T = Y_0^{\text{DCM}} \frac{3 + \exp(-2\gamma^{\text{DCM}}D_T) - \exp(-2\gamma^{\text{DCM}}L_{\text{TB}}) - 3\exp[-2\gamma^{\text{DCM}}(D_T + L_{\text{TB}})]}{3 - \exp(-2\gamma^{\text{DCM}}D_T) - \exp(-2\gamma^{\text{DCM}}L_{\text{TB}}) + 3\exp[-2\gamma^{\text{DCM}}(D_T + L_{\text{TB}})]}, \quad (24)$$

where L_{TB} is the length of the each branch given by $L_{\text{TB}} = (a_s - D_T)\theta_T$. Equation (24) is reduced to Eq. (19) under the condition $L_{\text{TB}} = 0$ relevant to the A-type models.

From Eqs. (13)-(24), we can obtain the low-frequency limits of $\overline{\varepsilon_s}$ and $\overline{\kappa_s}$ for both the LCM and DCM as

$$\overline{\varepsilon_s}^{\text{L}} = \varepsilon_s [1 + N_T L_{\text{TC}} / (\pi a_s)], \quad (25)$$

$$\overline{\kappa_s}^{\text{L}} = 0. \quad (26)$$

3. Results and discussion

3.1. Comparison between the EE- and the IE-type calculations

Figure 5 shows results of the EE- and the IE-type calculations for models S, C4, and A4-0580 that is the A-type model characterized by the following parameter values: $N_T = 4$, $W_T = 50$ nm, and $D_T = 8$ μm . In both types of the calculations, the dielectric spectrum for model A4-0580 includes two relaxation terms located around 100 kHz and 3 MHz. The high-frequency relaxation can be assigned to the β -relaxation due to the sarcolemma, because it coincides mostly with the relaxation exhibited by model S, in which the β -relaxation is expected from the approximate relations Eqs. (10) and (12). The low-frequency relaxation was affected by the structure of the T-tubules, as will be described in the following parts of this paper. Hence, this is attributable to the interfacial polarization in the T-tubules,

and is assigned to the α -relaxation. These assignments are consistent with those adopted by Fatt and Falk [10, 11]. Only the β -relaxation is found in the dielectric spectrum for model C4. This agrees with the results of the IE-type experiments for detubulated muscle fibers in which the connections between the sarcolemma and the T-tubules were disrupted [4, 21].

=== Fig. 4 ===

The two-step relaxation similar to that found in the dielectric spectra for model A4-0580 shown in Fig. 4 was provided by all the models examined in the present study, irrespective of the branching structure of the T-tubules in the B-type models. For further analyses of the effects of the T-tubules on the dielectric spectra, the α - and the β -relaxation were characterized by assuming the Cole-Cole type relaxation [42] as below:

$$\varepsilon_{\text{EED}}^* = \frac{\kappa_{\text{EED}}^{\text{L}}}{i\omega\varepsilon_0} + \frac{\varepsilon_{\text{EED}}^{\text{L}} - \varepsilon_{\text{EED}}^{\text{M}}}{1 + (i\omega\tau_{\text{EE}\alpha})^{m_{\text{EE}\alpha}}} + \frac{\varepsilon_{\text{EED}}^{\text{M}} - \varepsilon_{\text{EED}}^{\text{H}}}{1 + (i\omega\tau_{\text{EE}\beta})^{m_{\text{EE}\beta}}} + \varepsilon_{\text{EED}}^{\text{H}}, \quad (27)$$

$$C_{\text{IE}}^* = \frac{C_{\text{IE}}^{\text{L}} - C_{\text{IE}}^{\text{M}}}{1 + (i\omega\tau_{\text{IE}\alpha})^{m_{\text{IE}\alpha}}} + \frac{C_{\text{IE}}^{\text{M}} - C_{\text{IE}}^{\text{H}}}{1 + (i\omega\tau_{\text{IE}\beta})^{m_{\text{IE}\beta}}} + C_{\text{IE}}^{\text{H}}, \quad (28)$$

where m is the Cole-Cole parameter, the subscripts α and β refer to the α - and the β -relaxation, and the superscripts L, M, and H refer to the values at the low-frequency limit, between the α - and the β -relaxation, and at the high-frequency limit, respectively. The relaxation times $\tau_{\text{EE}\alpha}$, $\tau_{\text{EE}\beta}$, $\tau_{\text{IE}\alpha}$, and $\tau_{\text{IE}\beta}$ are, respectively, related to the relaxation frequencies $f_{\text{EE}\alpha}$, $f_{\text{EE}\beta}$, $f_{\text{IE}\alpha}$, and $f_{\text{IE}\beta}$ by relations of the following form: $\tau = 1/(2\pi f_0)$, where τ and f_0 are the relaxation time and the relaxation frequency, respectively.

To compare the behavior of the α -relaxation obtained from the EE-type calculations with that obtained from the IE-type ones, $f_{\text{EE}\alpha}$ is plotted against $f_{\text{IE}\alpha}$ in Fig. 5, and $\varepsilon_{\text{EED}}^{\text{L}}$ is plotted against C_{IE}^{L} in Fig. 6. As seen from Fig. 5, the relation between $f_{\text{EE}\alpha}$ and $f_{\text{IE}\alpha}$ can be represented as $f_{\text{EE}\alpha} = f_{\text{IE}\alpha}$. Figure 6 shows that $\varepsilon_{\text{EED}}^{\text{L}}$ varies in proportion to C_{IE}^{L} .

=== Fig. 5 ===

=== Fig. 6 ===

3.2. Comparisons between BEM and circuit model calculations

In addition to the numerical calculations with BEM, the calculations were carried out with the analytical relations for model S, in which ε_s^* was replaced by its equivalent quantity $\overline{\varepsilon_s^*}$, which is given by a relation $\overline{\varepsilon_s^*} = \overline{\varepsilon_s} + \overline{\kappa_s} / (i\omega\varepsilon_0)$, and Eqs. (13) and (14). The Y_T' and Y_T'' in Eqs. (13) and (14) were derived from the LCM or the DCM for the T-tubules described in sec. 2.3.

According to the approximate relations, Eqs. (10) and (12), for model S, $\varepsilon_{\text{EED}}'$ and C_{IE} for this model at frequencies much lower than the β -relaxation are represented as $\varepsilon_{\text{EED}}' = 4a_s\varepsilon_s/T_s$ and $C_{\text{IE}} = 2\pi\varepsilon_0(a_s\varepsilon_s/T_s)$, respectively. From these relations and Eq. (25) that is valid in both the LCM and the DCM, $\varepsilon_{\text{EED}}^L$ and C_{IE}^L are, respectively, represented by the relations $\varepsilon_{\text{EED}}^L = 4a_s\varepsilon_s^{-L}/T_s$ and $C_{\text{IE}}^L = 2\pi\varepsilon_0(a_s\varepsilon_s^{-L}/T_s)$. Hence, the relation between $\varepsilon_{\text{EED}}^L$ and C_{IE}^L is expected to be represented as $\varepsilon_{\text{EED}}^L/C_{\text{IE}}^L = 2/(\pi\varepsilon_0)$. This relation is shown in Fig. 6 by a solid line, which agrees with the plots obtained from the BEM calculations. This result suggests the validity of the circuit models in explaining the behavior of the α -relaxation at the low-frequency limit.

Calculations of $\varepsilon_{\text{EED}}^*$ and C_{IE}^* with the DCM were carried out using Eqs. (3)-(8), (13), and (14), where Y_T was evaluated from Eq. (19) in the case of the A-type models, and from Eq. (24) in the case of the B-type ones. Frequency dependence of $\varepsilon_{\text{EED}}'$ and that of C_{IE} for model A4-0580 obtained with DCM following this procedure are shown in Fig. 4. It is seen from Fig. 4(A) that the DCM was successful in explaining the behavior of $\varepsilon_{\text{EED}}^*$ for model A4-0580 evaluated with BEM at frequencies around $f_{\text{EE}\alpha}$. However, the DCM provided a slight deviation from the results of the BEM calculations at frequencies around $f_{\text{EE}\beta}$; this is attributable to the T-tubules perpendicular to the external electric fields, as will be discussed in sec. 3.3. In the case of C_{IE}^* shown in Fig. 4(B), the DCM was successful in the whole frequency region examined in the present study. Similar results were obtained in the case of the B-type models with the branched T-tubules (data are not shown).

In the calculations with the LCM, it is required to determine reasonable values of the access resistance R_A^{LCM} of the T-tubules. As a trial, R_A^{LCM} was represented as follows under the assumption that R_A^{LCM} is attributed to the whole T-tubule in the A-type models, and to the part of the T-tubule between the mouth and the branch point in the B-type models:

$$R_A^{\text{LCM}} = D_T / (W_T \kappa_a). \quad (29)$$

Using Eqs. (18) and (29), Eq. (17) can be rewritten as:

$$f_T^{\text{LCM}} = T_s W_T \kappa_a / (4\pi L_{TC} D_T \varepsilon_s \varepsilon_0). \quad (30)$$

Figure 7 shows the relations between $f_{EE\alpha}$ and f_T^{LCM} . In the case of the A-type models, there was a linear relation between $f_{EE\alpha}$ and f_T^{LCM} represented as $f_{EE\alpha} = 2.3 f_T^{\text{LCM}}$. This suggests that $f_{EE\alpha}$ is essentially explained by the LCM with the morphological parameters of the T-tubule although R_A is overestimated. The relation $f_{EE\alpha} = 2.3 f_T^{\text{LCM}}$ leads to a relation

$$R_A^{\text{LCM}} = D_T / (W_T \kappa_a) / 2.3 = 0.43 D_T / (W_T \kappa_a). \quad (31)$$

In the case of the B-type models, most of the data points are located near the solid line representing the relation $f_{EE\alpha} = f_T^{\text{LCM}}$. This suggests that the R_A^{LCM} for the branched T-tubules is attributable to the part of the T-tubules between the mouth and the branch point. Since $f_{IE\alpha} = f_{EE\alpha}$ as shown in Fig. 5, the same relations for the A- and the B-type models are expected to be valid in the results of the IE-type calculations. The frequency dependence of ε_{EED}' and that of C_{IE} for model A4-0580 obtained with the LCM are also shown in Fig. 4.

=== Fig. 7 ===

3.3. Results of the EE-type calculations for models A2 and B2

In the models with four or eight T-tubules (models A4, A8, B4 and C4), the components of $\varepsilon_{\text{EED}}^*$ along the x - and the y -axis are equal to each other, i.e., $\varepsilon_{\text{EED}x}^* = \varepsilon_{\text{EED}y}^*$. In addition to these models, we examined the case of $\varepsilon_{\text{EED}x}^* \neq \varepsilon_{\text{EED}y}^*$ using models with only two T-tubules along the x -axis (models A2 and B2). In this case, $\varepsilon_{\text{EED}x}^*$ contained both the α - and the β -relaxation, whereas $\varepsilon_{\text{EED}y}^*$ did only the β -relaxation. Table 2 shows the relaxation parameters specified in Eq. (27) for $\varepsilon_{\text{EED}x}^*$ and $\varepsilon_{\text{EED}y}^*$ of models A2-0595 ($N_T = 2$, $W_T = 50$ nm, and $D_T = 9.5$ μm) and those of B2-238 ($N_T = 2$, $W_T = 50$ nm, $D_T = 9.5$ μm , and $\theta_T = 3.8\pi/16$). For comparison, this table includes the parameter values for model S without the T-tubules, and those for models A4-0595 and B4-238 that have four T-tubules of the same morphology as in A2-0595 and B2-238, respectively. The relaxation parameters related to the α -relaxation ($\varepsilon_{\text{EED}}^L$, $\varepsilon_{\text{EED}}^M$, $f_{\text{EE}\alpha}$, and $m_{\text{EE}\alpha}$) suggest that the behavior of the α -relaxation in $\varepsilon_{\text{EED}x}^*$ of models A2-0595 and B2-238 is the same as that in $\varepsilon_{\text{EED}x}^*$ and $\varepsilon_{\text{EED}y}^*$ ($\varepsilon_{\text{EED}x}^* = \varepsilon_{\text{EED}y}^*$) of models A4-0595 and B4-238. This indicates that the occurrence of the α -dispersion depends on the direction of the T-tubules, and that its relaxation intensity has the maximum when the T-tubules are connected to the surface at right angles to the external fields. In addition, values of the relaxation parameters for the β -relaxation ($\varepsilon_{\text{EED}}^M$, $\varepsilon_{\text{EED}}^H$, $f_{\text{EE}\beta}$, and $m_{\text{EE}\beta}$) suggest that the T-tubules affect the β -relaxation, and that the effects are also dependent on the direction. The effects of the field direction on the β -relaxation are more complicated than those on the α -relaxation. For example, $f_{\text{EE}\beta}$, and $m_{\text{EE}\beta}$ along the y -axis are smaller than those along the x -axis in the case of model A2-0595, whereas the opposite relations are found in model B2-238. In model A2-0595, the T-tubules are straight and are placed along the x -axis. On the other hand, the T-tubules in model B2-238 have long branches that are mostly directed along the y -axis. These indicate that the portions of the T-tubules perpendicular to the external fields cause the decreases in $f_{\text{EE}\beta}$ and $m_{\text{EE}\beta}$.

3.4. Comparison with experimental results

Figure 5 has shown that the relation $f_{\text{EE}\alpha} = f_{\text{IE}\alpha}$ holds between the relaxation frequencies of the α -relaxation $f_{\text{EE}\alpha}$ and $f_{\text{IE}\alpha}$ obtained, respectively, from the EE- and the IE-type calculations. This result is consistent with the observations that the α -relaxation is found at frequencies near 100 Hz in both

types of the experiments [4, 5]. However, the values of $f_{EE\alpha}$ and $f_{IE\alpha}$ obtained in the present study are much larger than the observed values. In the EE-type experiments [1, 5], the relaxation frequencies of the α - and the β -relaxation are about 100 Hz and 300 kHz, respectively. As seen from Fig. 4(A), values of these relaxation frequencies obtained in the present study are estimated as follows: $f_{EE\alpha} = 85$ kHz in the case of model A4-0580, and $f_{EE\beta} = 4.4$ MHz in model S. The discrepancy between the experimental and the theoretical values is attributable, in part, to the values of T_s ($T_s = 10$ nm) and ε_s ($\varepsilon_s = 2$) used in the present study. The membrane capacitance C_M for the shell phase in the present study is evaluated as $C_M = \varepsilon_0 \varepsilon_s / T_s = 1.8 \cdot 10^{-3}$ F/m². This value is about 1/15 of the C_M -values accepted for the cell membrane of the skeletal muscles [4, 5, 21]. This means that the values of ε_s / T_s in the real cells are about 15 times as large as that in the present study. According to Eqs. (10), (12), (20)-(22), effects of ε_s / T_s on the dielectric spectra can be represented by a term that includes the frequency as $\omega \varepsilon_s / T_s$. This suggests that the increase in ε_s / T_s causes the same effects as the decrease in frequency. Hence, the following values are expected in the calculations using the realistic values of ε_s / T_s : $f_{IE\alpha} = f_{EE\alpha} = 85$ kHz/15 = 5.7 kHz for model A4-0580, and $f_{EE\beta} = 4.4$ MHz/15 = 290 kHz for model S. The corrected value of $f_{EE\beta}$ ($f_{EE\beta} = 290$ kHz) is in good agreement with experimental results. On the other hand, the corrected value of $f_{EE\alpha}$ ($f_{EE\alpha} = 5.7$ kHz) is still much larger than the experimental results. Since $f_{EE\alpha}$ is significantly affected by the T-tubule structure, as shown in the present study, the unsuccessful estimation of $f_{EE\alpha}$ is attributable to the oversimplified structure of the T-tubules examined in the present study.

Figure 6 has shown that ε_{ED}^L varies in proportion with C_{IE}^L with the proportional coefficient independent of the cell structure. This result is consistent with the conventional assumption about the relation between the results of the EE-type experiments and those of the IE-type ones, derived from the circuit models for the T-tubules. This suggests that the deformation of the cell membrane due to the T-tubule structure in a single skeletal muscle cell is not helpful in explaining the excess in the intensity of the α -relaxation observed in the EE-type experiments over that expected from the IE-type ones. Beside the counterion polarization proposed by Schwan [1, 5], modification of the interfacial polarization due to electrical interactions between the muscle fibers is expected to be one of the

candidates for the mechanism available to explain the disagreements between the observations and the theoretical results in the present study, and is needed to be examined in future studies.

Symbols in the text

Structure and electrical properties of models

a_s	radius of circular region in models
c_T^{DCM}	specific capacitance of T-tubule membrane in distributed-circuit model (DCM)
C_M	membrane capacity for the shell phase, $C_M = \varepsilon_0 \varepsilon_s / T_s$
C_T^{LCM}	capacitance of T-tubule membrane in limped-circuit model (LCM)
d_T	space between shell phase and T-tubule in model C4
D_T	depth of T-tubule toward the circle center
f	frequency of external field and applied voltage
f_T^{LCM}	relaxation frequency for T-tubule in LCM
i	imaginary unit
L_{TC}	length of T-tubule in xy -plane, $L_{TC} = D_T + 2(a_s - D_T)\theta_T$
L_{TB}	length of each branch of T-tubule, $L_{TB} = (a_s - D_T)\theta_T$
r_L^{DCM}	specific resistance of tubular lumen
R_A^{LCM}	access resistance of T-tubule in LCM
S	area of model
T_s	thickness of shell phase
W_T	width of T-tubule
Y_0^{DCM}	$= 1 / Z_0^{\text{DCM}}$
Y_T	admittance of T-tubule
Z_0^{DCM}	characteristic impedance of T-tubule in DCM
γ^{DCM}	propagation constant of T-tubule in DCM
ε_0	permittivity of vacuum

$\varepsilon_a, \varepsilon_i, \text{ and } \varepsilon_s$	relative permittivity of outer, inner, and shell phases
$\varepsilon_a^*, \varepsilon_i^*, \text{ and } \varepsilon_s^*$	complex permittivity of outer, inner, and shell phases
$\overline{\varepsilon_s}$	equivalent permittivity of shell phase
$\overline{\varepsilon_s}^*$	equivalent complex permittivity of shell phase
$\overline{\varepsilon_s}^L$	low-frequency limit of $\overline{\varepsilon_s}$
$\kappa_a, \kappa_i, \text{ and } \kappa_s$	conductivity of outer, inner, and shell phases
$\overline{\kappa_s}$	equivalent conductivity of shell phase
$\overline{\kappa_s}^L$	low-frequency limit of $\overline{\kappa_s}$
θ_T	azimuth of branch of T-tubule in models B2 and B4
τ_T^{LCM}	relaxation time for T-tubule in LCM
ω	angular frequency; $\omega = 2\pi f$

Calculations relevant to extracellular electrode (EE) method

$B_{\text{EE}x} \text{ and } B_{\text{EE}y}$	complex polarization factors of model along x- and y-axis
$\mathbf{E}_{\text{EE}0}(E_{\text{EE}0x}, E_{\text{EE}0y})$	external electric field
$f_{\text{EE}\alpha} \text{ and } f_{\text{EE}\beta}$	relaxation frequencies of α - and β -relaxation
$m_{\text{EE}\alpha} \text{ and } m_{\text{EE}\beta}$	Cole-Cole parameters of α - and β -relaxation
P	area fraction of two-dimensional suspension of models
$\mathbf{r}(x, y)$	position around the model where ϕ_{EE} is examined
v	area fraction of inner phase within shelled circle for model S
$\varepsilon_{\text{EE}}^*$	complex permittivity of two-dimensional suspension of models
$\varepsilon_{\text{EED}}' \text{ and } \varepsilon_{\text{EED}}''$	real part of $\varepsilon_{\text{EED}}^*$ and imaginary part of $\varepsilon_{\text{EED}}^*$ except for contribution of κ_{EED}^L
$\varepsilon_{\text{EED}}^L, \varepsilon_{\text{EED}}^M \text{ and } \varepsilon_{\text{EED}}^H$	$\varepsilon_{\text{EED}}'$ at low-frequency limit, between α - and β -relaxation, and at high-frequency limit
$\varepsilon_{\text{EED}}^*$	normalized increment in complex permittivity due to models in suspension

$\varepsilon_{\text{EEDx}}^*$ and $\varepsilon_{\text{EEDy}}^*$	$\varepsilon_{\text{EED}}^*$ due to oriented models along x- and y-axis
ε_{q}^*	equivalent complex permittivity of shelled circle for model S
$\kappa_{\text{EED}}^{\text{L}}$	dc conductivity in $\varepsilon_{\text{EED}}^*$
$\tau_{\text{EE}\alpha}$ and $\tau_{\text{EE}\beta}$	relaxation times of α - and β -relaxation
ϕ_{EE}	induced potential at $\mathbf{r}(x, y)$

Calculations relevant to intracellular electrode (IE) method

a_{IEH} and a_{IEG}	radius of circles corresponding to internal electrode and ground
C_{IE} and G_{IE}	capacitance and conductance for model of unit length along z-axis
C_{IE}^{L} , C_{IE}^{M} and C_{IE}^{H}	C_{IE} at low-frequency limit, between α - and β -relaxation, and at high-frequency limit
C_{IE}^*	complex capacitance for model of unit length along z-axis
$f_{\text{IE}\alpha}$ and $f_{\text{IE}\beta}$	relaxation frequencies of α - and β -relaxation
I_{IEH}	electric current per unit length along z-axis through internal electrode
$m_{\text{IE}\alpha}$ and $m_{\text{IE}\beta}$	Cole-Cole parameters of α - and β -relaxation
V_{IEH} and V_{IEG}	external voltage at circles corresponding to internal electrode and ground

Appendix A. Admittance of T-tubules derived from the distributed circuit model

According to the transmission line theory, the propagation of the voltage and the current waves in the T-tubules in the A-type models is represented by the following relations:

$$V_{\text{T}}(l) = V_{\text{F}}\exp(-\gamma^{\text{DCM}}l) + V_{\text{B}}\exp(\gamma^{\text{DCM}}l), \quad (\text{A1})$$

$$I_{\text{T}}(l) = Y_0^{\text{DCM}}[V_{\text{F}}\exp(-\gamma^{\text{DCM}}l) - V_{\text{B}}\exp(\gamma^{\text{DCM}}l)], \quad (\text{A2})$$

where γ^{DCM} and Y_0^{DCM} are represented by Eqs. (20) and (21) in the text, respectively, and l is the distance from the cell surface. In the calculations of Y_{T} , we assumed that the waves are perfectly

reflected at the bottom of the tubules, namely,

$$V_T(D_T) = 0. \quad (\text{A3})$$

Since the current that flows through each of the T-tubules causes the difference between $I_T(0)$ and $I_T(D_T)$, the Y_T for the T-tubules is given by the following relation using the difference in I_T and the voltage difference across the T-tubule membrane at the cell surface, $V_T(0)$:

$$Y_T = [I_T(0) - I_T(D_T)] / V_T(0). \quad (\text{A4})$$

From Eqs. (A1)-(A4), we obtain Eq. (19).

In the case of the B-type, the voltage and the current waves from the cell surface to the branch point ($0 \leq l \leq D_T$), V_{T1} and I_{T1} , and those in the branches ($D_T \leq l \leq D_T + L_{TB}$), V_{T2} and I_{T2} , are represented as

$$V_{T1}(l) = V_{F1} \exp(-\gamma^{\text{DCM}} l) + V_{B1} \exp(\gamma^{\text{DCM}} l), \quad (\text{A5})$$

$$I_{T1}(l) = Y_0^{\text{DCM}} [V_{F1} \exp(-\gamma^{\text{DCM}} l) - V_{B1} \exp(\gamma^{\text{DCM}} l)], \quad (\text{A6})$$

$$V_{T2}(l) = V_{F2} \exp(-\gamma^{\text{DCM}} l) + V_{B2} \exp(\gamma^{\text{DCM}} l), \quad (\text{A7})$$

$$I_{T2}(l) = Y_0^{\text{DCM}} [V_{F2} \exp(-\gamma^{\text{DCM}} l) - V_{B2} \exp(\gamma^{\text{DCM}} l)]. \quad (\text{A8})$$

The following conditions are required for the continuity of the voltage and the current at the branch point ($l = D_T$):

$$V_{T1}(D_T) = V_{T2}(D_T), \quad (\text{A9})$$

$$I_{T1}(D_T) = 2I_{T2}(D_T). \quad (\text{A10})$$

Similarly to Eq. (A3), at the bottom of the T-tubules,

$$V_{T2}(D_T + L_{TB}) = 0. \quad (\text{A11})$$

The Y_T for the B-type models is given as

$$\begin{aligned} Y_T &= \{[I_{T1}(0) - I_{T1}(D_T)] + 2[I_{T2}(D_T) - I_{T2}(D_T + L_{TB})]\} / V_{T1}(0) \\ &= [I_{T1}(0) - 2I_{T2}(D_T + L_{TB})] / V_{T1}(0). \end{aligned} \quad (\text{A12})$$

Using Eqs. (A5)-(A11), Eq. (A12) is modified into Eq. (24) in the text.

References

- [1] H.P. Schwan, Electrical properties of tissue and cell suspensions, in: J.H. Lawrence, C.A. Tobias (Eds.), *Advances in Biological and Medical Physics*, vol. 5, Academic Press, New York, 1957, pp. 147-209.
- [2] K.S. Cole, *Membranes, Ions and Impulses*, University of California Press, Berkeley, Los Angeles, 1968
- [3] R. Pethig, D.B. Kell, The passive electrical properties of biological systems: their significance in physiology, biophysics and biotechnology, *Phys. Med. Biol.*, 32 (1987) 933-970.
- [4] S. Takashima, *Electrical Properties of Biopolymers and Membranes*, Adam Hilger, Bristol, Philadelphia, 1989
- [5] K.R. Foster, H.P. Schwan, Dielectric properties of tissues, in: C. Polk, E. Postow (Eds.), *Handbook of Biological Effects of Electromagnetic Fields*, 2nd ed., CRC Press, Boca Raton, New York, London, Tokyo, 1996, pp. 25-102.
- [6] C. Gabriel, S. Gabriel, E. Corthout, The dielectric properties of biological tissues: I. Literature survey, *Phys. Med. Biol.*, 41 (1996) 2231-2249.
- [7] B. Rigaud, J.-P. Morucci, N. Chauveau, Bioelectrical impedance techniques in medicine Part I: Bioimpedance measurement, second section: Impedance spectrometry, *Crit. Rev. Biomed. Eng.*, 24 (1996) 257-351.
- [8] K. Asami, Dielectric relaxation spectroscopy of biological cell suspensions, in: V.A. Hackley, J. Texter (Eds.), *Handbook on Ultrasonic and Dielectric Characterization Techniques for Suspended Particulates*, The American Ceramic Society, Westerville, 1998, pp. 333-349.
- [9] T.J.C. Faes, H.A. van der Meij, J.C. de Munck, R.M. Heethaar, The electric resistivity of human tissues (100 Hz-10 MHz): A meta- analysis of review studies, *Physiol. Meas.*, 20 (1999) R1-R10.
- [10] P. Fatt, An analysis of the transverse electrical impedance of striated muscle, *Proc. R. Soc. London. Ser. B*, 159 (1964) 606-651.
- [11] G. Falk, P. Fatt, Linear electrical properties of striated muscle fibers observed with intracellular electrodes, *Proc. R. Soc. London. Ser. B*, 160 (1964) 69-123.
- [12] E. Gersing, Impedance spectroscopy of living tissue for determination of the state of organs,

- Bioelectrochem. Bioenerg., 45 (1998) 145-149.
- [13] E.C. Fear, M.A. Stuchly, Modeling assemblies of biological cells exposed to electric fields, IEEE Trans. Biomed. Eng., 45 (1998) 1259-1271.
- [14] K. Asami, Dielectric dispersion of erythrocyte ghosts, Phys. Rev. E, 73 (2006) 052903.
- [15] H.M. Fishman, D. Poussart, L.E. Moore, E. Siebenga, K^+ conduction description from the low frequency impedance and admittance of squid axon, J. Membr. Biol., 32 (1977) 255-290.
- [16] H.M. Fishman, D. Poussart, L.E. Moore, Complex admittance of Na^+ conduction in squid axon, J. Membr. Biol., 50 (1979) 43-63.
- [17] L.A. Dissado, A fractal interpretation of the dielectric response of animal tissues, Phys. Med. Biol., 35 (1990) 1487-1503.
- [18] H.P. Schwan, Determination of biological impedance, In: W.L. Nastuk (Ed.), Physical Techniques in Biological Research, vol. 6 pt. B, Academic Press, New York, 1963, pp. 323-407.
- [19] C. Grosse, M.C. Tirado, Low-frequency dielectric spectroscopy of colloidal suspensions, J. Non-Cryst. Solids, 305 (2002) 386-392.
- [20] R.H. Adrian, Electrical properties of striated muscle, in: L.D. Peachey, R.H. Adrian, S.R. Geiger (Eds.), Handbook of Physiology, sect. 10, American Physiological Society, Bethesda, 1983, pp. 275-300.
- [21] R.S. Eisenberg, Impedance measurement of the electrical structure of skeletal muscle, in: L.D. Peachey, R.H. Adrian, S.R. Geiger (Eds.), Handbook of Physiology, sect. 10, American Physiological Society, Bethesda, 1983, pp. 301-323.
- [22] H.P. Schwan, Die elektrischen Eigenschaften von Muskelgewebe bei Niederfrequenz, Z. Naturforsch., 9b (1954) 245-251.
- [23] C.T. O'Konski, Effect of interfacial conductivity on dielectric properties, J. Chem. Phys. 23 (1955) 1559.
- [24] H. Pauly, H.P. Schwan, Über die Impedanz einer Suspension von kugelförmigen Teilchen mit einer Schale, Z. Naturforsch., 14b (1959) 125-131.
- [25] M. Saito, H.P. Schwan, G. Schwarz, Response of nonspherical biological particles to alternating electric fields, Biophys. J., 6 (1966) 313-327.

- [26] K. Asami, T. Hanai, N. Koizumi, Dielectric approach to suspensions of ellipsoidal particles covered with a shell in particular reference to biological cells, *Jpn. J. Appl. Phys.*, 19 (1980) 359-365.
- [27] T. Kakutani, S. Shibutani, M. Sugai, Electrorotation of non-spherical cells: Theory for ellipsoidal cells with an arbitrary number of shells, *Bioelectrochem. Bioenerg.*, 31 (1993) 131-145.
- [28] B.J. Roth, F.L.H. Gielen, J.P. Wikswo Jr., Spatial and temporal frequency-dependent conductivities in volume-conduction calculations for skeletal muscle, *Math. Biosci.*, 88 (1988) 159-189.
- [29] E. Tuncer, Y.V. Serdyuk, S.M. Gubanski, Dielectric mixtures: Electrical properties and modeling, *IEEE Trans. Dielec. Elec. Insul.*, 9 (2002) 809-828.
- [30] C. Brosseau, A. Beroual, Computational electromagnetics and the rational design of new dielectric heterostructures, *Prog. Mat. Sci.*, 48 (2003) 373-456.
- [31] F.L.H. Gielen, H.E.P. Cruts, B.A. Albers, K.L. Boon, W. Wallinga-de Jonge, H.B.K. Boom, Model of electrical conductivity of skeletal muscle based on tissue structure, *Med. Biol. Eng. Comput.*, 24 (1986) 34-40.
- [32] B.R. Eisenberg, Quantitative ultrastructure of mammalian skeletal muscle, in: L.D. Peachey, R.H. Adrian, S.R. Geiger (Eds.), *Handbook of Physiology*, sect. 10, American Physiological Society, Bethesda, 1983, pp. 73-112.
- [33] Laboratory for Insulation Research, Massachusetts Institute of Technology, Tables of dielectric materials, in: A. von Hippel (Ed.), *Dielectric Materials and Applications*, 2nd edn., Artech House, Boston, 1995, pp. 291-433.
- [34] P. Vanýsek, Equivalent conductivity of electrolytes in aqueous solution, in: D.R. Lide (Ed.), *CRC Handbook of Chemistry and Physics*, 79th edn., CRC Press, Boca Raton, 1998, p. 5-92.
- [35] K. Sekine, Application of boundary element method to calculation of the complex permittivity of suspensions of cells in shape of $D_{\infty h}$ symmetry, *Bioelectrochem.*, 52 (2000) 1-7.
- [36] K. Sekine, N. Torii, C. Kuroda, K. Asami, Calculation of dielectric spectra of suspensions of rod-shaped cells using boundary element method, *Bioelectrochem.*, 57 (2002) 83-87.
- [37] K. Sekine, C. Kuroda, N. Torii, Boundary-element calculations for dielectric relaxation of

water-in-oil-in-water emulsions consisting of spherical droplets with a spheroidal core, *Colloid Polym. Sci.*, 280 (2002) 71-77.

[38] K. Sekine, Y. Watanabe, S. Hara, K. Asami, Boundary-element calculations for dielectric behavior of doublet-shaped cells, *Biochi. Biophys. Acta*, 1721 (2005) 130-138.

[39] M.H. Lean, M. Friedman, A. Wexler, Application of the boundary element method in electrical engineering problems, in: P.K. Banerjee, R. Butterfield (Eds.), *Developments in Boundary Element Methods-1*, Elsevier Applied Science Publishers, New York, 1979, pp. 207-250.

[40] C.A. Brevvia, *The Boundary Element Method for Engineers*, 2nd edn., Pentech Press, London, 1980.

[41] J.A. Stratton *Electromagnetic Theory*, McGraw-Hill, New York, 1941

[42] K.S. Cole, R.H. Cole, Dispersion and absorption in dielectrics, *J. Chem. Phys.*, 9 (1941) 341-351.

Table 1

Vales of morphological parameters for the T-tubules to examine effects of tubular structure on dielectric spectra

parameters	N_T	W_T/nm	$D_T/\mu\text{m}$	$\theta_T/(\pi/16)$
changed				
Models A2, A4, A8 (straight T-tubules)				
N_T	4, 8	50	8	0
N_T	2, 4	50	9.5 ^{*)}	0
W_T	4	50, 100, 200	8	0
D_T	4	50	4, 6, 8	0
D_T	8	50	4, 6, 8	0
Models B2, B4 (branched T-tubules)				
N_T	2, 4	50	2	3.8
D_T	4	50	1, 2, 3	3.8
θ_T	4	50	2	1, 2, 3, 3.8

^{*)} used only in EE-type calculations

Table 2

Effects of the direction k of the external electric field on the relaxation parameters for $\varepsilon_{\text{EED}k}^*$ for models A2-0595 and A4-0595 ($D_T = 9.5 \mu\text{m}$, $W_T = 50 \text{ nm}$), and B2-238 and B4-238 ($D_T = 2 \mu\text{m}$, $W_T = 50 \text{ nm}$, $\theta_T = 3.8\pi/16$), parameter values for model S being shown for comparison

Model	k	$\frac{-\kappa_{\text{EED}}^{\text{L}}}{\text{S/m}}$	$\frac{\varepsilon_{\text{EED}}^{\text{L}}}{10^4}$	$\frac{\varepsilon_{\text{EED}}^{\text{M}}}{10^3}$	$-\varepsilon_{\text{EED}}^{\text{H}}$	$\frac{f_{\text{EE}\alpha}}{\text{kHz}}$	$\frac{f_{\text{EE}\beta}}{\text{MHz}}$	$m_{\text{EE}\alpha}$	$m_{\text{EE}\beta}$
A4-0595	x, y	1.00	0.87	4.87	3.24	60	1.70	1.00	0.78
A2-0595	x	1.00	0.87	4.44	1.55	66	3.49	0.97	0.94
A2-0595	y	1.00	-	3.20	3.26	-	2.70	-	0.86
B4-238	x, y	1.00	1.10	4.53	3.98	58	1.68	1.00	0.79
B2-238	x	1.00	1.10	4.38	3.31	59	2.43	1.00	0.87
B2-238	y	1.00	-	3.20	2.19	-	3.88	-	0.94
S	x, y	1.00	-	3.92	1.57	-	4.41	-	1.00

Figure Captions

Fig. 1. Two-dimensional models for the cross section of a skeletal muscle fiber. Circles in bold lines are shells corresponding to sarcolemma. Bold lines in the circles represent the invaginations of the shell representing the T-tubules.

Fig. 2. Models for the structure of the T-tubules.

Fig. 3. Equivalent circuit models for the T-tubules. (A) Lumped circuit model (LCM): C_T^{LCM} , the capacitance of the T-tubule membrane; R_A^{LCM} , the access resistance. (B) Distributed circuit model (DCM): c_T^{DCM} , the capacitance of the T-tubule membrane; r_L^{DCM} , the resistance of the T-tubule lumen per unit length.

Fig. 4. Dielectric spectra for models S, C4, and A4-0580 (A-type in which $N_T = 4$, $W_T = 50$ nm, and $D_T = 8$ μm) obtained from the calculations relevant to experiments with (A) extracellular electrode (EE) method and (B) intracellular electrode (EE) method. Open (\circ) and filled (\bullet) circles are data points for models A4-0580 and C4, respectively, calculated with BEM. Three solid lines refer to the curves obtained analytically for model S, and for model A4-0580 with the circuit models, LCM and DCM, as indicated in the figure.

Fig. 5. Relation between the relaxation frequencies of the α -relaxation obtained from the IE-type BEM calculations, $f_{\text{IE}\alpha}$, and those obtained from the EE-type ones, $f_{\text{EE}\alpha}$. The solid line represents the relation $f_{\text{EE}\alpha} / f_{\text{IE}\alpha} = 1$.

Fig. 6. Relation between the low-frequency limit C_{IE}^{L} obtained from the IE-type BEM calculations and that $\varepsilon_{\text{EED}}^{\text{L}}$ obtained from the EE-type ones. The solid line represents the relation $\varepsilon_{\text{EED}}^{\text{L}} / C_{\text{IE}}^{\text{L}} = 2 / (\pi \varepsilon_0)$.

Fig. 7. The $f_{\text{EE}\alpha}$ compared with the relaxation frequency f_T^{LCM} for the T-tubule obtained from the LCM. The f_T^{LCM} values were calculated assuming that the access resistance R_A^{LCM} was attributed to the whole tubule in A-type models, and to the tubule between the mouth and the branch point in B-type models.

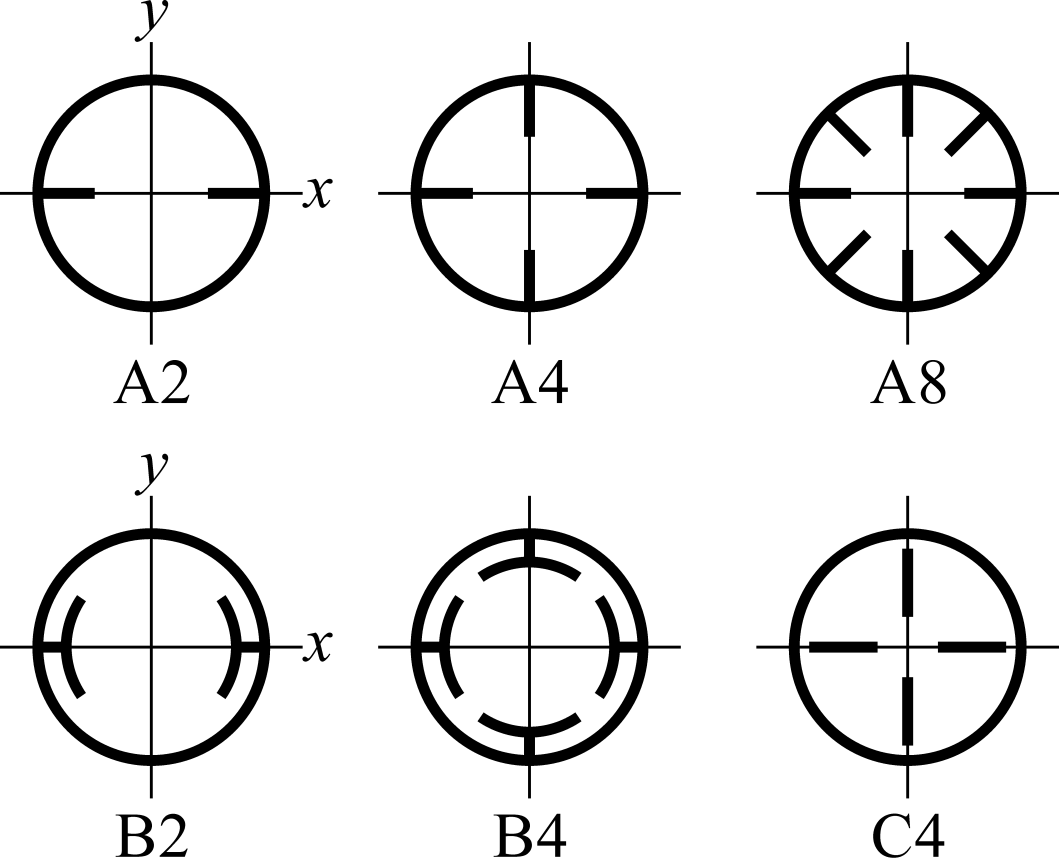


Fig. 1. K. Sekine

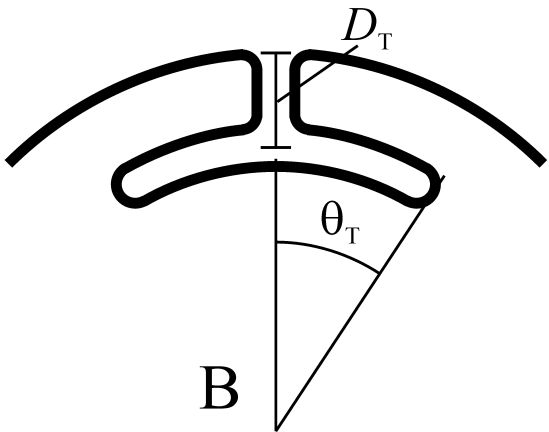
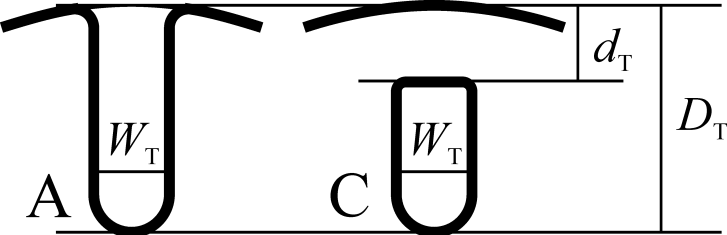
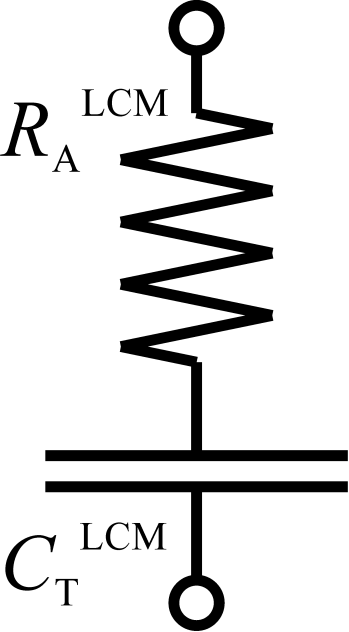
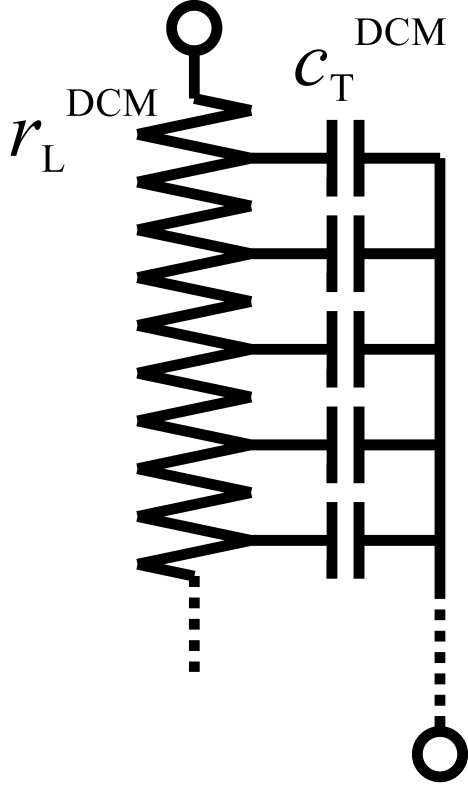


Fig.2. K. Sekine



(A) LCM



(B) DCM

Fig. 3. K. Sekine

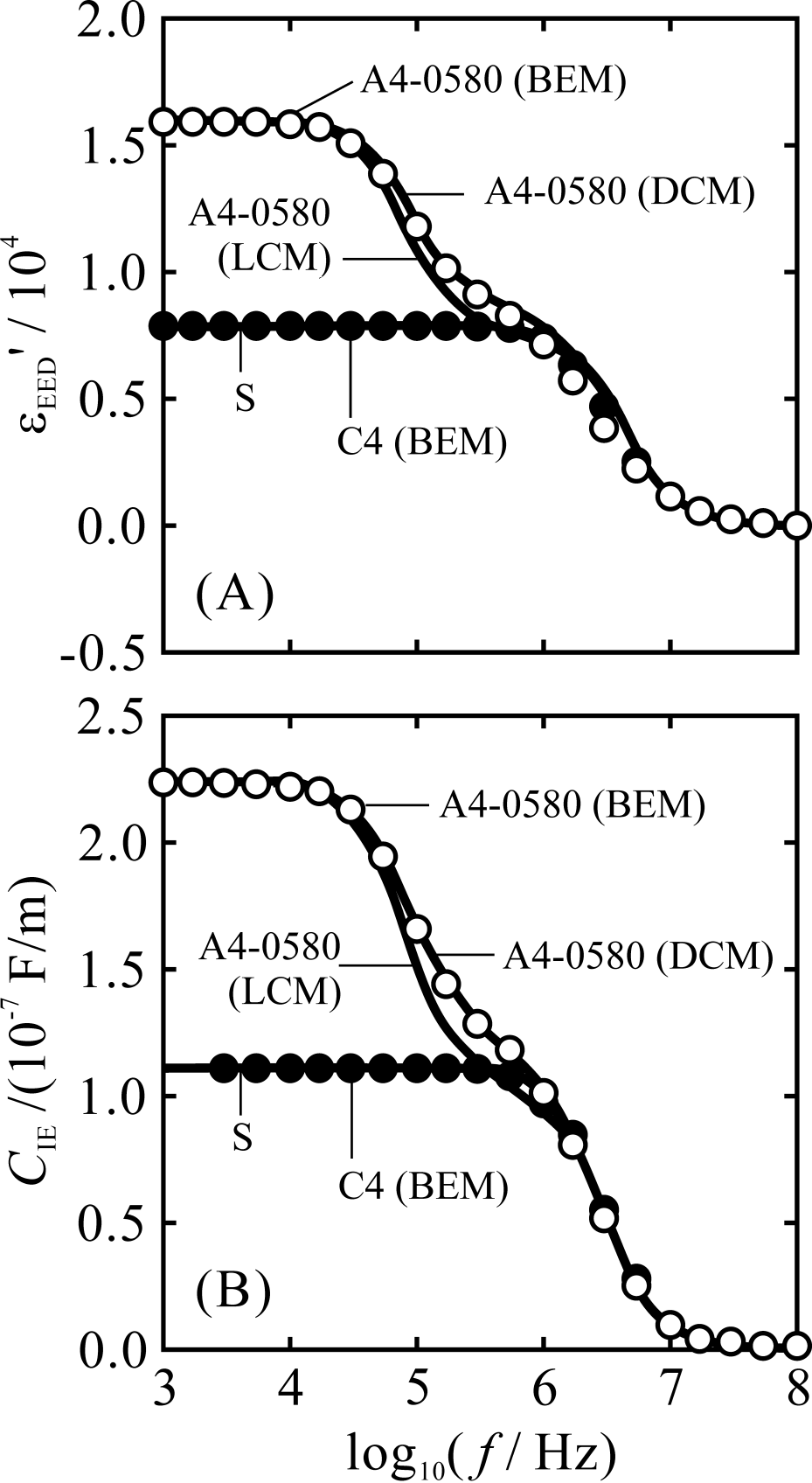


Fig. 4. K. Sekine

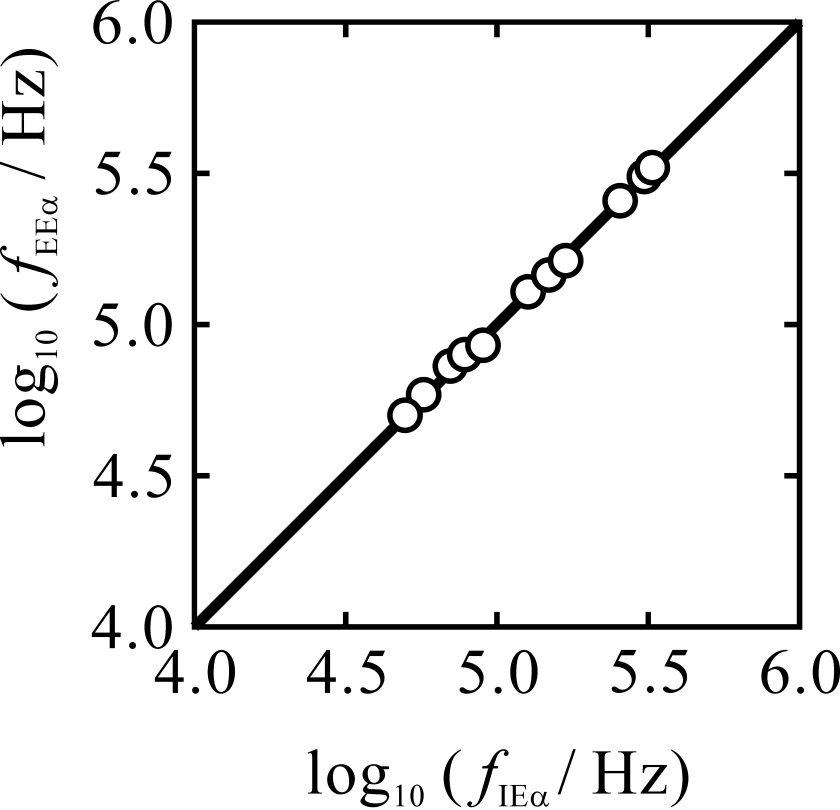


Fig. 5. K. Sekine

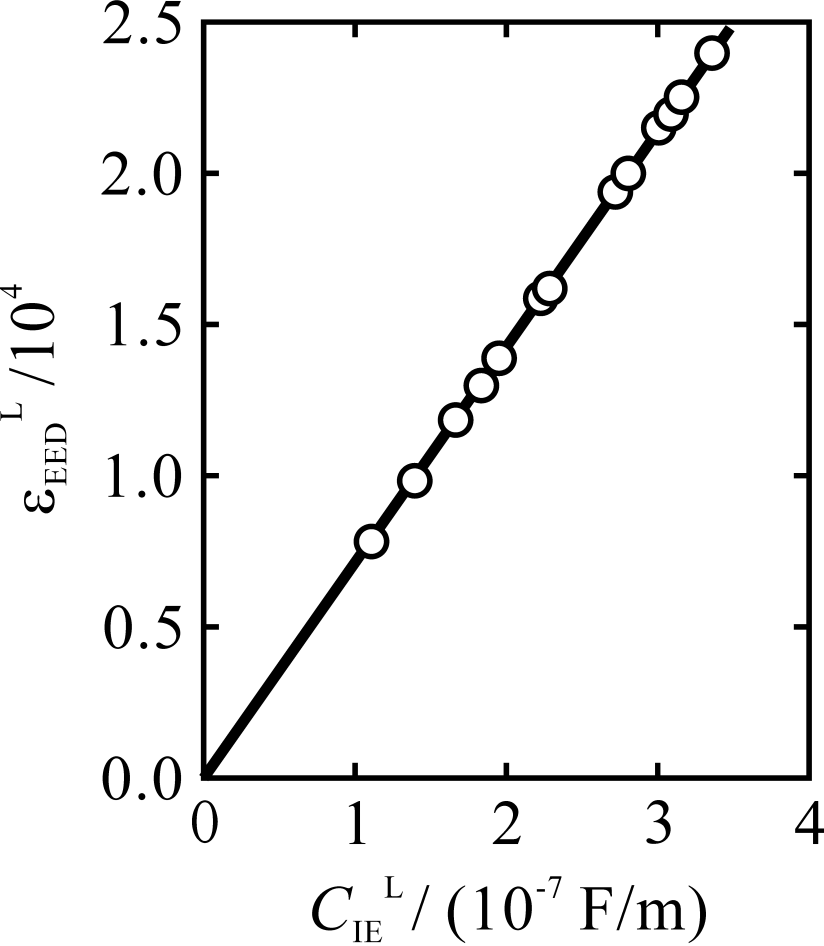


Fig. 6. K. Sekine

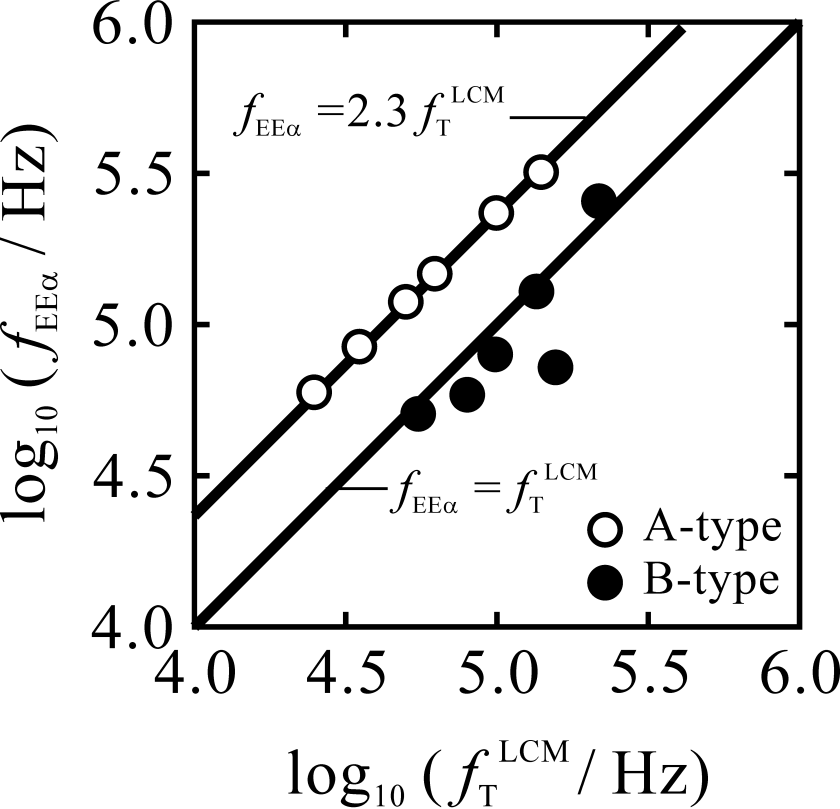


Fig. 7. K. Sekine